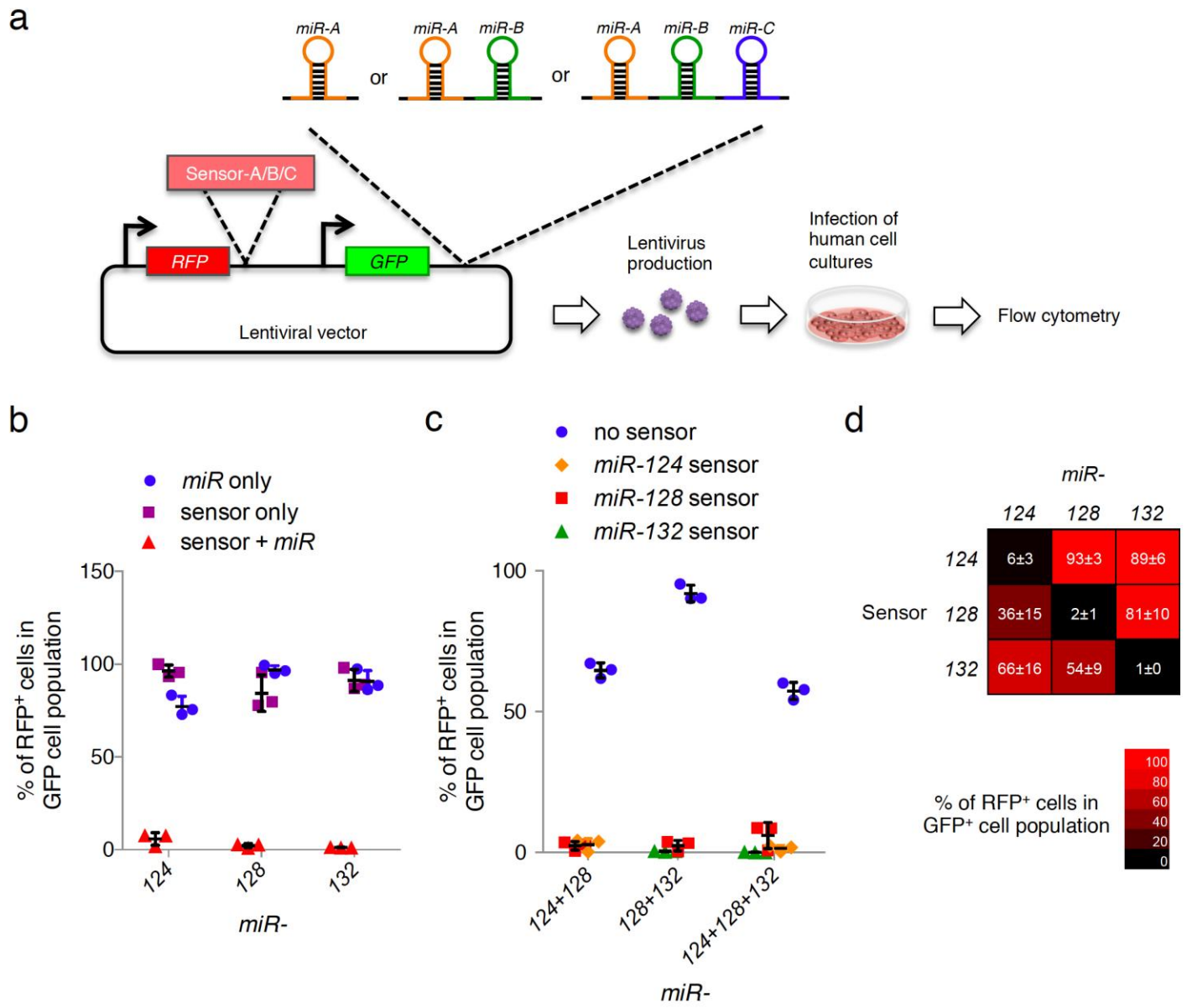

Supplementary Figure 1

Lentiviral Delivery of Combinatorial miRNA Expression Constructs Provides Efficient Target Gene Repression.

a, Design for lentiviral combinatorial miRNA expression and sensor constructs. Single or multiple miRNA precursor sequences arranged in tandem were placed downstream of a *GFP* gene to monitor expression driven by a CMV promoter in a lentiviral vector. Sensors harboring four repeats of the miRNA target sequence were cloned in the 3'UTR of a *RFP* gene expressed from an UBC promoter to report on miRNA activity. The constructs were delivered by lentiviruses to HEK293T cells and then analyzed for GFP and RFP expression using flow cytometry. **b,** Repression of RFP reporter activity by miRNA expression. Lentiviral constructs harboring a miRNA, the cognate sensor, or both were introduced into HEK293T cells. **c,** Combinatorial miRNA expression constructs effectively repressed RFP reporters containing the cognate miRNA sensors. Lentiviral constructs harboring two-wise or three-wise miRNA combinations, with or without the cognate sensors, were introduced into HEK293T cells. **d,** Limited cross-reactivity between miRNAs and non-cognate sensors. Lentiviral constructs harboring miRNAs paired with different sensors were delivered into HEK293T cells. The percentages of RFP-positive cells within GFP-positive cell populations were determined by flow cytometry. Data represent mean ± s.d. (n = 3).

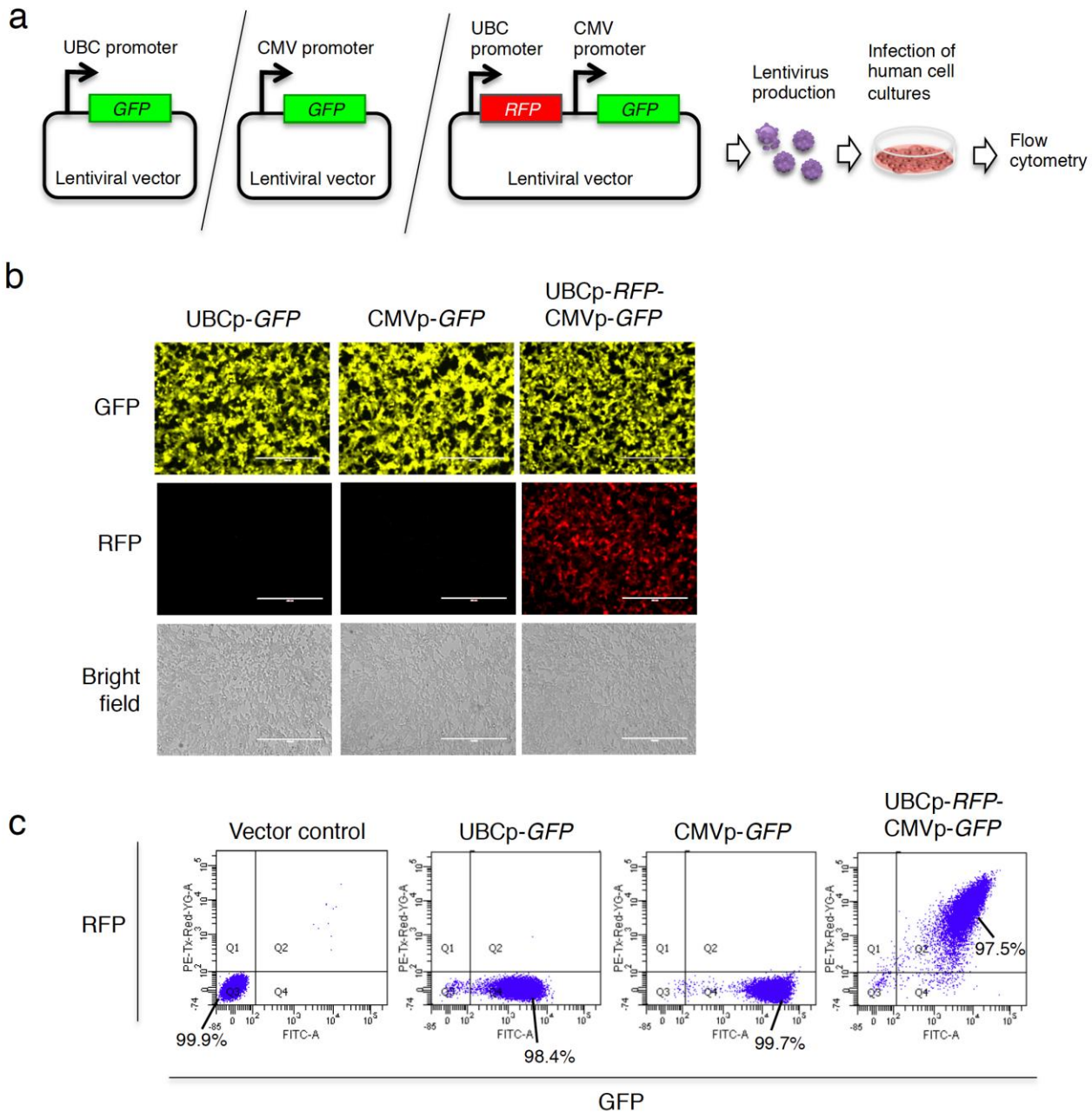

Supplementary Figure 2

Efficient Lentiviral Delivery of a Dual-Fluorescent Protein Reporter Construct in Human Cells.

a, Strategy for testing lentiviral delivery of a dual-fluorescent protein reporter construct in human cells. Lentiviruses generated for vectors containing a *GFP* gene expressed from a CMV or UBC promoter, or a single vector encoding *RFP* and *GFP* genes under the UBC and CMV promoters, respectively, were delivered to HEK293T cells for analysis of GFP and RFP expression. **b, c,** Lentiviral delivery and expression of the dual-fluorescent protein reporter construct in human cells. (**b**) Fluorescent microscopy revealed that RFP and GFP were expressed in UBCp-*RFP*-CMVp-*GFP* virus-infected cells, whereas only GFP was expressed in cells infected with UBCp-*GFP* and CMVp-*GFP* lentiviruses. Scale bar denotes 400 μm. (**c**) Flow cytometry was used to measure cell populations positive for RFP and GFP fluorescence. Over 97 percent of UBCp-*RFP*-CMVp-*GFP* virus-infected HEK293T cells were positive for both RFP and GFP, and similar percentages of UBCp-*GFP* or CMVp-*GFP* virus-infected cells were GFP-positive.

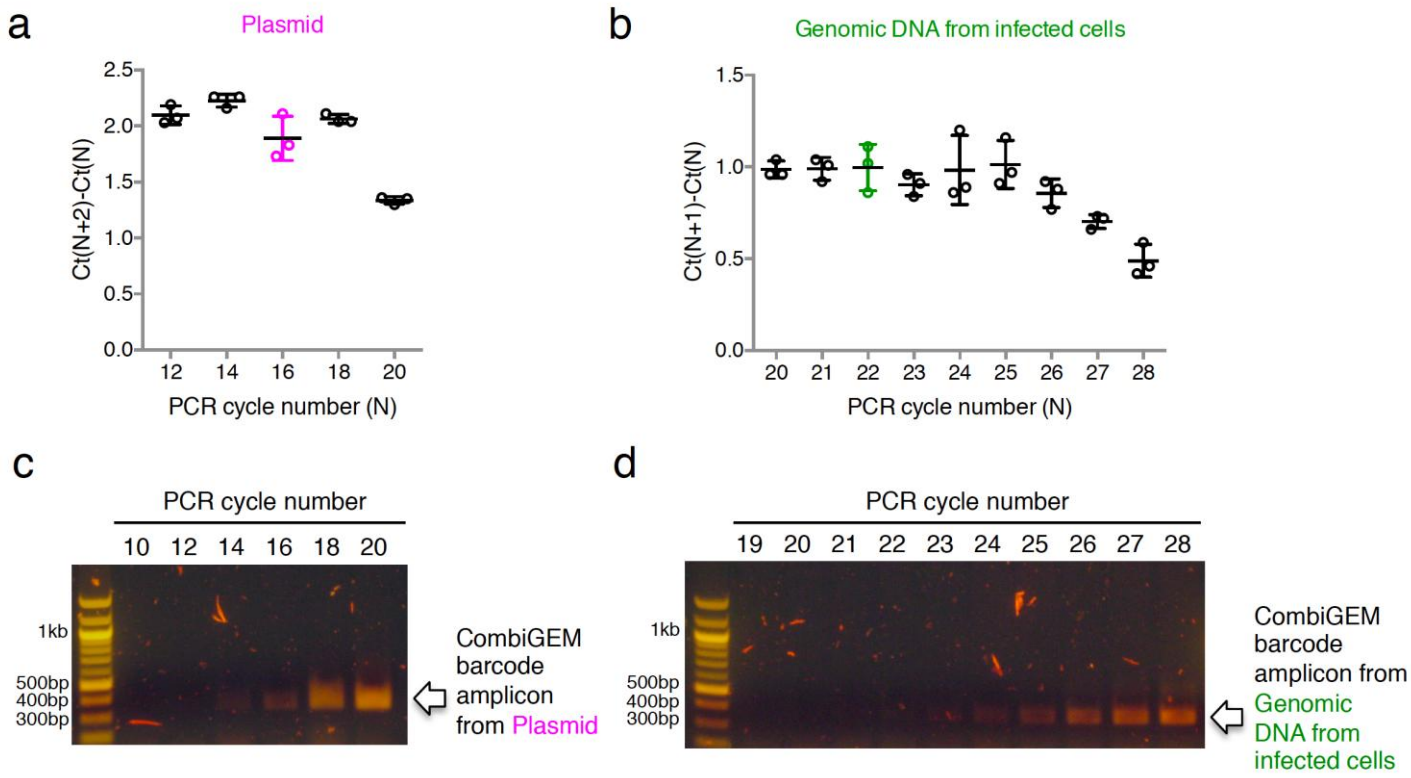

Supplementary Figure 3

Identification of the Exponential Phase During PCR for CombiGEM Barcode Amplification.

a, b, Procedures for identifying the transition point from exponential to linear phase during PCR for CombiGEM barcode amplification. The one-wise miRNA vector library pooled-assembled in *E. coli* (**a**) and the genomic DNA isolated from human breast cancer cells (MCF7) infected with the two-wise library (**b**) were used as templates in replicate PCR reactions, and the barcodes representing each miRNA combinations were amplified using primers targeting the sequences located outside the barcode region. PCR products were collected from the reactions stopped at cycles between 10 to 20 (**a**) or 19 to 28 (**b**), and were then diluted as templates for quantitative PCR reactions. The mean difference of threshold cycle (Ct) between cycles was determined. Error bars indicate s.d. from triplicates. Primer efficiencies were estimated to be 102% (**a**) and 100% (**b**) respectively. PCR cycle numbers highlighted in magenta (**a**) and green (**b**) were used in unbiased barcode amplification for subsequent Illumina sequencing. **c, d,** Agarose gel analyses of the amplified PCR products with indicated cycle numbers from (**a**) and (**b**) are shown in (**c**) and (**d**), respectively.

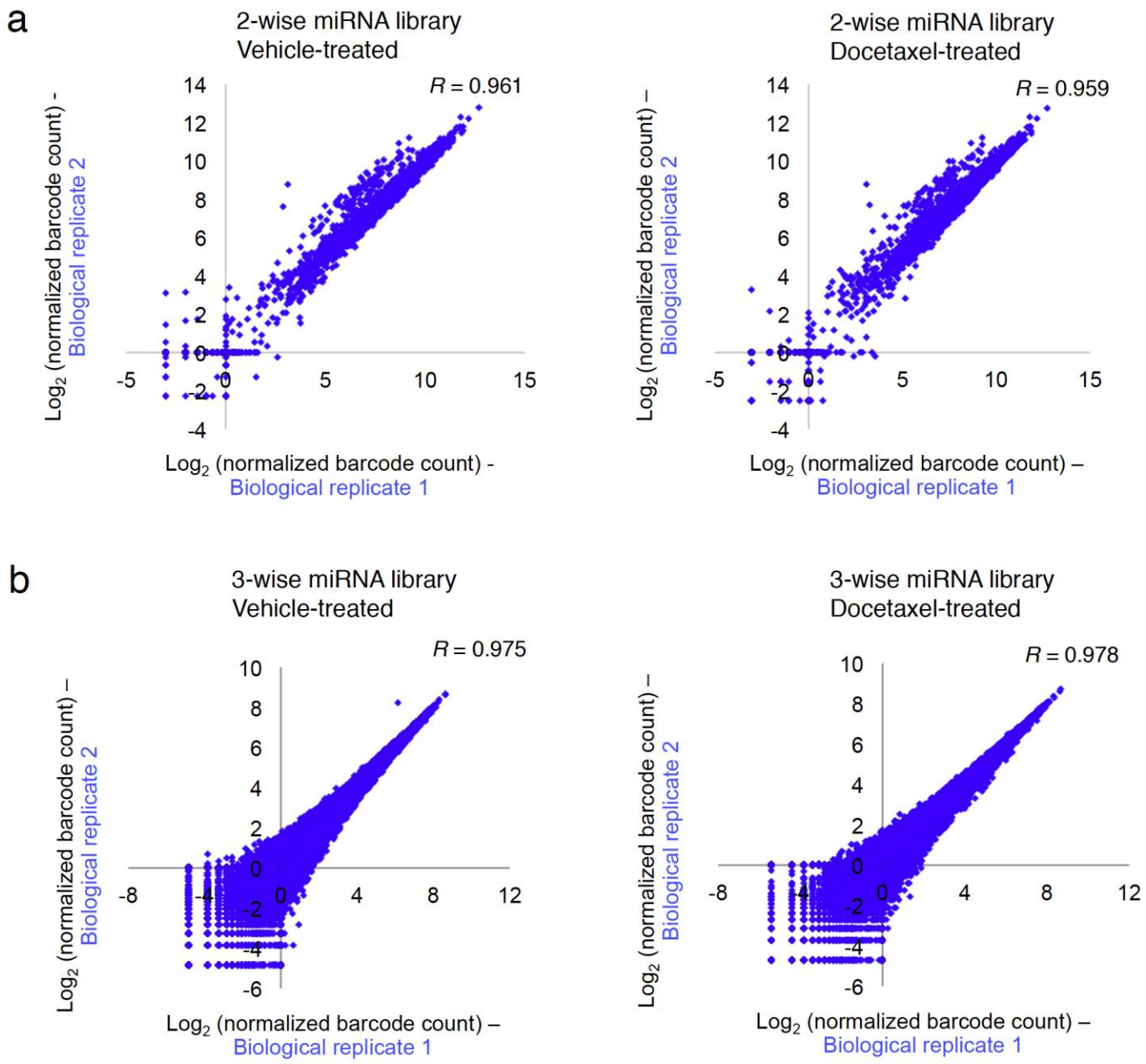

Supplementary Figure 4

High Reproducibility of Barcode Quantitation in Biological Replicates for Combinatorial miRNA Screens.

a, b, Scatter plots showing high correlation between barcode representations (log_2 number of normalized barcode counts) between two biological replicates for both docetaxel (25 nM)-treated or vehicle-treated OVCAR8-ADR cells infected with the two-wise (**a**) or three-wise (**b**) miRNA combinatorial libraries. *R* is Pearson correlation coefficient.

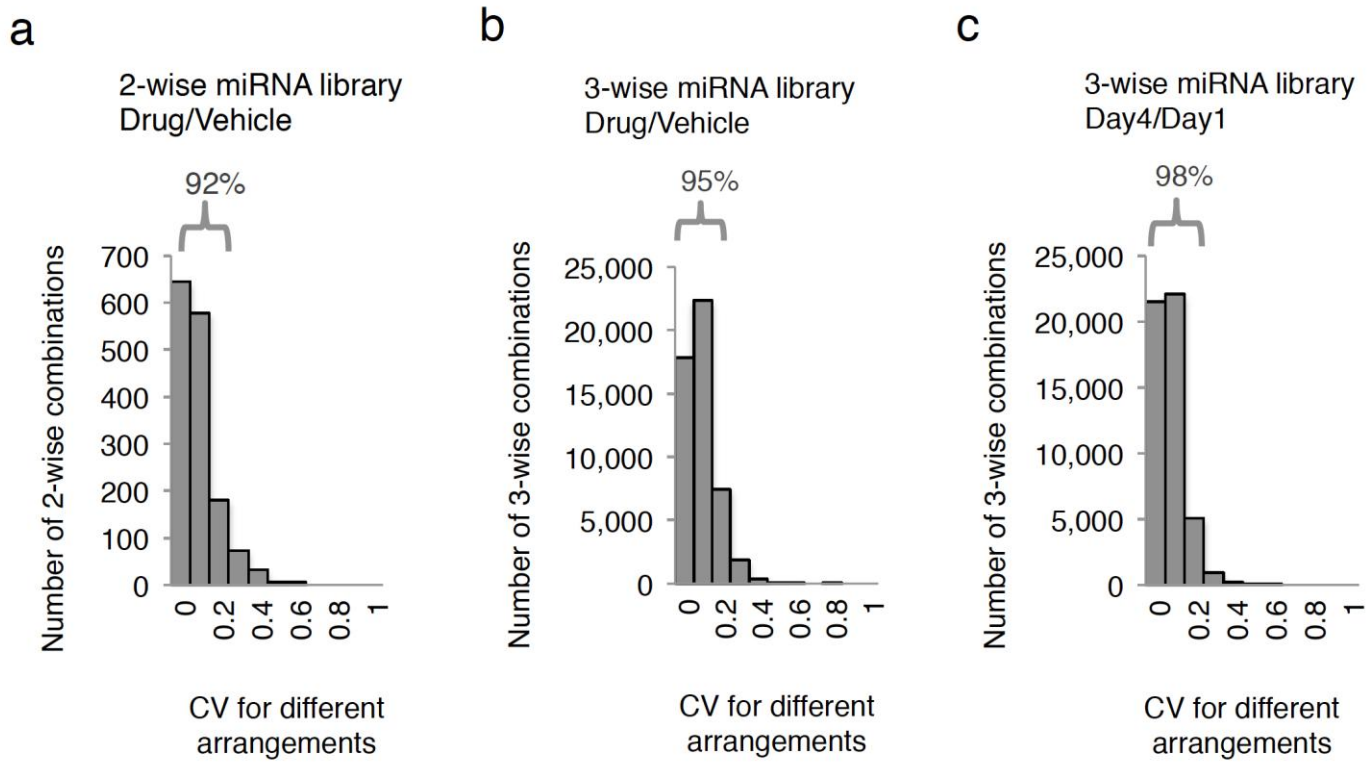

Supplementary Figure 5

Consistent Fold Changes of Barcodes among Same miRNA Combinations Arranged in Different Orders in the Expression Constructs.

a-c, The coefficient of variation (CV; defined as s.d./mean of the fold changes of normalized barcode counts for docetaxel (25 nM)-treated versus four-day vehicle-treated (**a, b**) and four-day versus one-day cultured cells (**c**)) was determined for the same two-wise (**a**) or three-wise (**b, c**) combination arranged in different orders (i.e., [A,B] vs. [B,A] for two-wise combinations; [A,B,C], [A,C,B], [B,A,C], [B,C,A], [C,A,B], and [C,B,A] for three-wise combinations). 92% of two-wise miRNA combinations had a CV of <0.2 in the drug-sensitivity screen (**a**), while 95% and 98% of three-wise combinations showed a CV of <0.2 in the drug-sensitivity (**b**) and cell-proliferation (**c**) screens respectively.

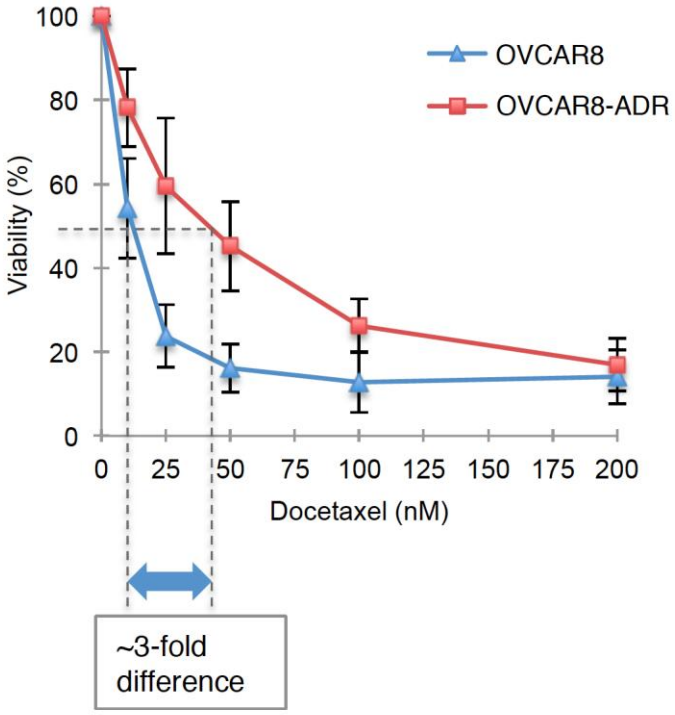

Supplementary Figure 6

Docetaxel Dose-Response Curves for the OVCAR8 Cell Line and the Docetaxel-Resistant OVCAR8-ADR Cell Line.

OVCAR8 cells and OVCAR8-ADR cells (OVCAR8's docetaxel-resistant derivative) cells were treated with docetaxel at indicated doses for three days and subjected to the MTT assay. Cell viabilities were compared to their respective no drug controls. The OVCAR8-ADR cell line has a ~3-fold higher IC_{50} than the parental OVCAR8 cell line. Data represent mean ± s.d. (n = 3).

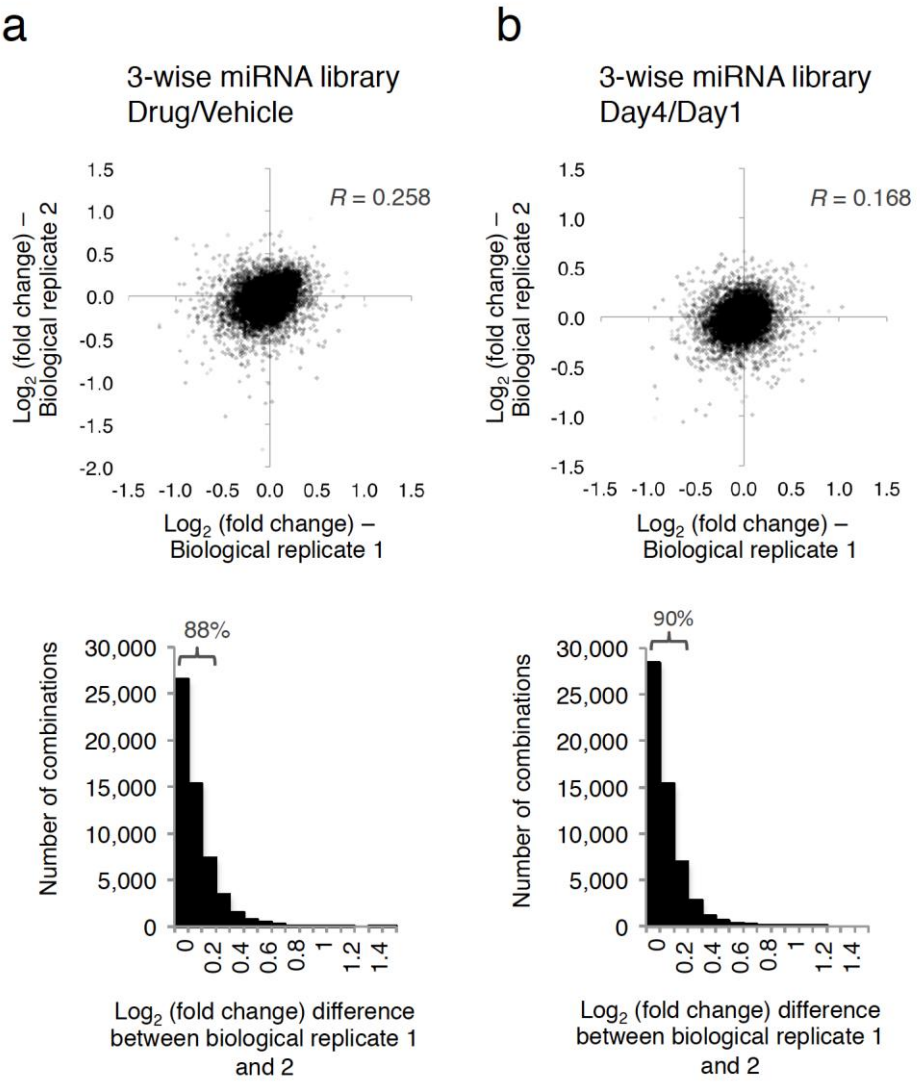

Supplementary Figure 7

Log_2 Fold-Changes in Barcode Representation Between Biological Replicates for All Individual Combinations in the Pooled Screens.

a, b (upper panel), Log_2 fold-changes in biological replicate 1 is plotted against replicate 2 for mean values of normalized barcode counts for docetaxel (25 nM)-treated versus vehicle-treated OVCAR8-ADR cells (a), and for relative cell viability at day 4 versus day 1 (b), for each three-wise combination. **a, b (lower panel),** Distributions of differences in the log_2 fold change between two biological replicates at a bin size of 0.1 are shown. A majority of three-wise combinations (88-90%) had <0.3 log_2 fold-change differences. *R* is the Pearson correlation coefficient.

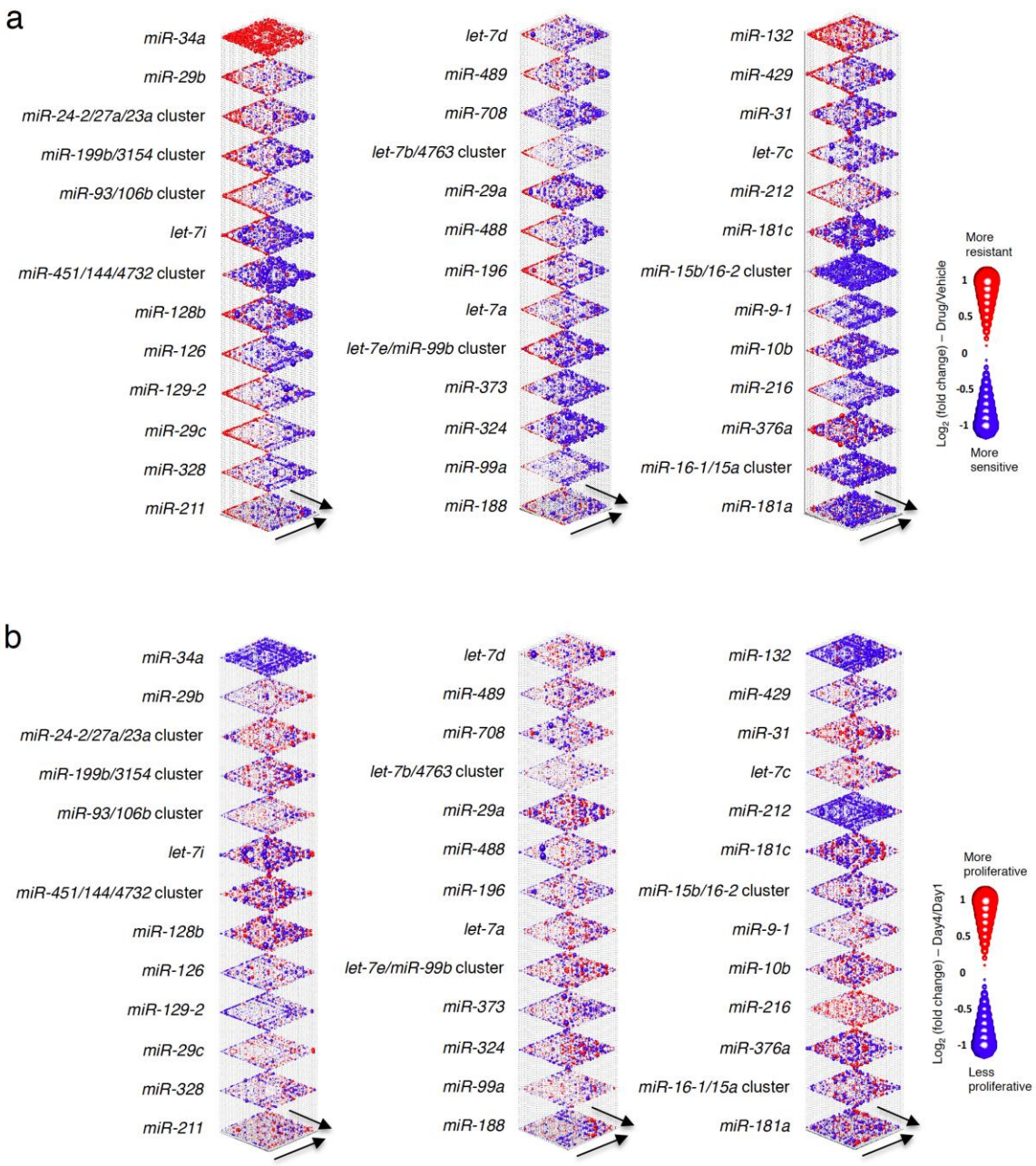

Supplementary Figure 8

Three-dimensional Plots Depicting the Docetaxel-Sensitizing (**a**) and Proliferation-Modulating (**b**) Effects of Three-Wise miRNA Combinations.

The $\log_2$ ratios of the normalized barcode counts for docetaxel-treated versus four-day vehicle-treated OVCAR8-ADR cells (**a**) or four-day versus one-day cultured cells (**b**) were determined for all three-wise miRNA combinations, and were presented as colored bubbles. miRNA combinations with drug-resistance and drug-sensitization effects (**a**) have $\log_2$ ratios >0 and <0, respectively, and those with pro-proliferation and anti-proliferation effects (**b**) have $\log_2$ ratios >0 and <0, respectively. Each two-dimensional plane was arranged in the same hierarchically clustered order as in (**Fig. 5a-c**), and the additional third miRNA element is labeled. All $\log_2$ ratios shown were determined from the mean of two biological replicates.

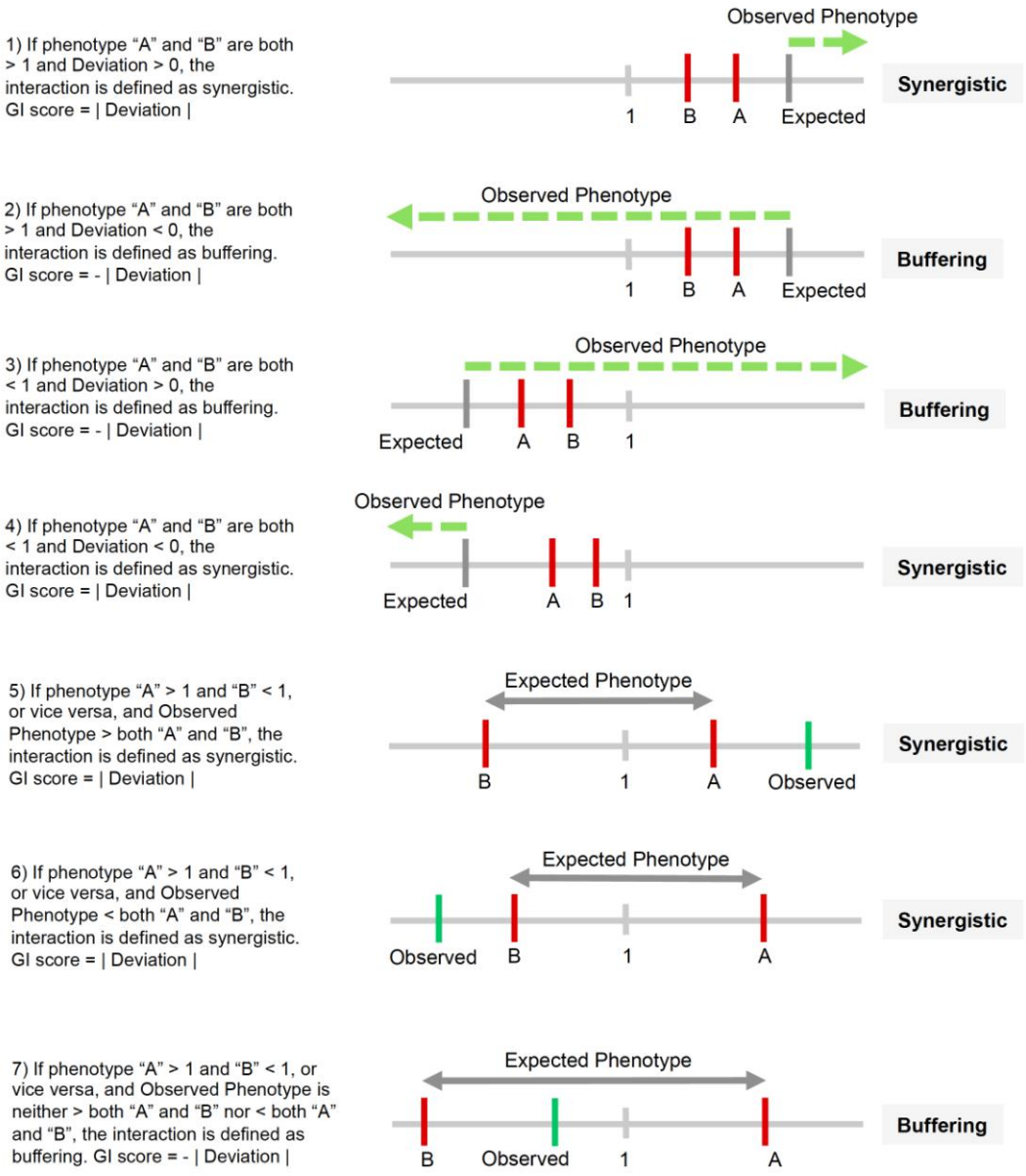

Supplementary Figure 9

Definitions of Genetic Interactions (GIs) in This Study.

Synergistic or buffering interactions have positive and negative GI scores, respectively, as described for case 1 to 7 in this figure. Positive and negative phenotypes have fold-changes of normalized barcode reads of >1 and <1 respectively, while no phenotype corresponds to a fold-change = 1. For miRNAs [A] and [B] with individual phenotypes "A" and "B", the expected phenotype for the two-wise combination [A,B] is ("A" + "B" - 1) according to the additive model. Deviation was calculated by subtracting the expected phenotype from observed phenotype (i.e., Observed phenotype – Expected phenotype).

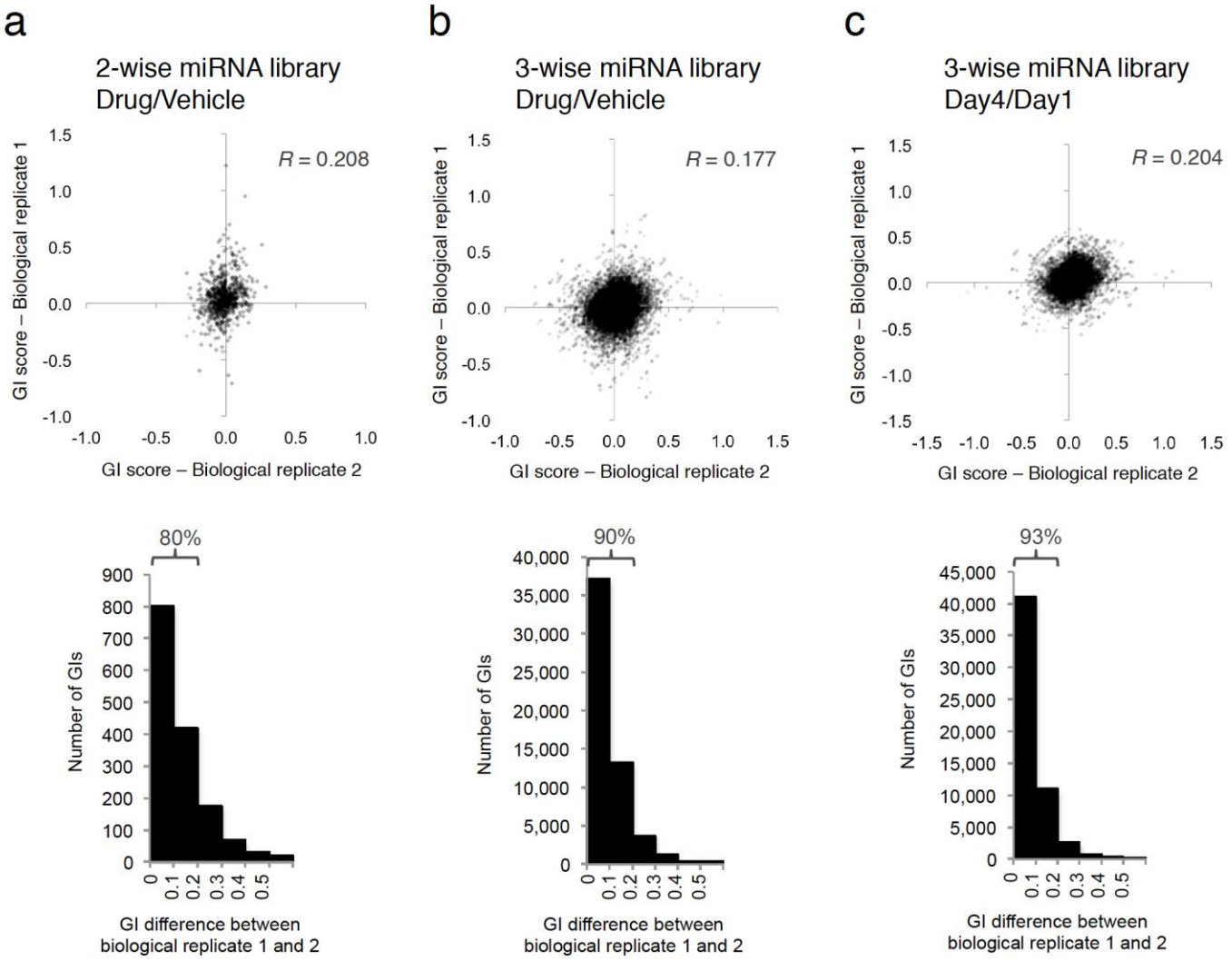

Supplementary Figure 10

GI Scores Between Biological Replicates for All Individual Combinations in the Pooled Screens.

a-c (upper panel), GI scores in biological replicate 1 are plotted against replicate 2 for docetaxel (25 nM)-treated versus vehicle-treated OVCAR8-ADR cells for each two-wise combination (**a**) and three-wise miRNA combination (**b**) respectively, and for relative cell viability at day 4 versus day 1 for each three-wise combination (**c**). **a-c (lower panel),** Distributions of differences in the GI scores between two biological replicates at a bin size of 0.1 are shown. A majority of combinations (80-93%) had GI score differences of <0.2.

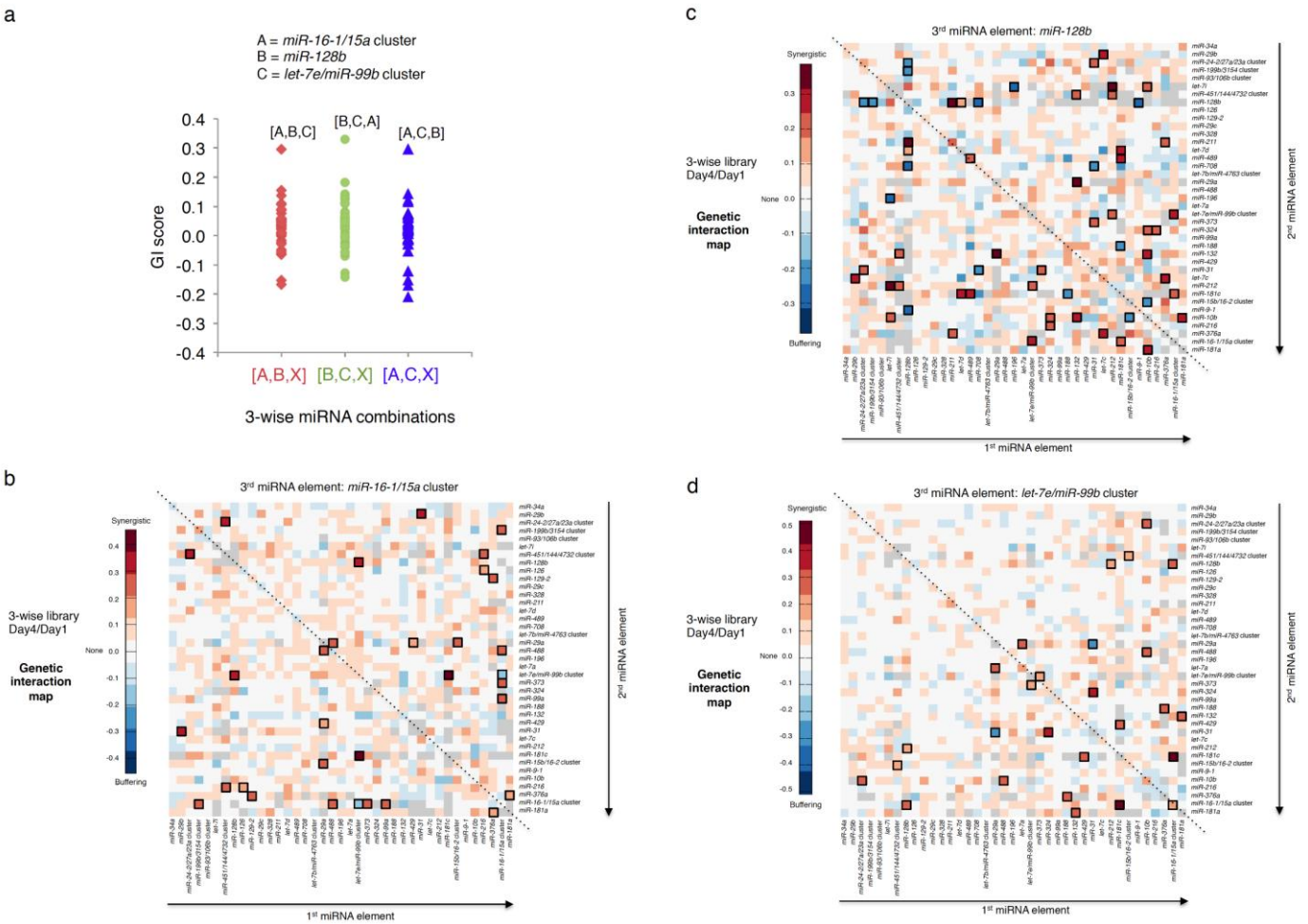

Supplementary Figure 11

Synergistic Interactions between the *miR-16-1/15a* Cluster, *miR-128b*, and the *let-7e/miR-99b* Cluster Modulate Cell Proliferation Phenotypes.

a, GI scores for a given three-wise miRNA combination [A,B,C] are plotted and compared to other combinations that harbor two of the same miRNAs (in the first two positions) and every other miRNA member in our library (denoted as X in the third position). GI scores of each three-wise miRNA combination were calculated as described in **Online Methods,** and represent the interaction between the additional third miRNA and the two-wise miRNA combinations. GI scores were determined for the three possible permutations (i.e., [A,B,C], [B,C,A], and [A,C,B], see **Online Methods**). In this example, A, B, and C represent the *miR-16-1/15a* cluster, *miR-128b*, and the *let-7e/miR-99b* cluster respectively, and X represents all 39 library members. **b-d,** GI maps based on cell-proliferation phenotypes for all three-wise miRNA combinations harboring the *miR-16-1/15a* cluster, *miR-128b*, and/or the *let-7e/miR-99b* cluster are displayed in the same order as for the GI map in **Fig. 5a** for easy comparison, with the additional third miRNA element in the three-wise combination being labeled above each GI map. The combinations for which no GIs were measured are indicated in gray. The combinations with GI at a Q-value of <0.003 are boxed.

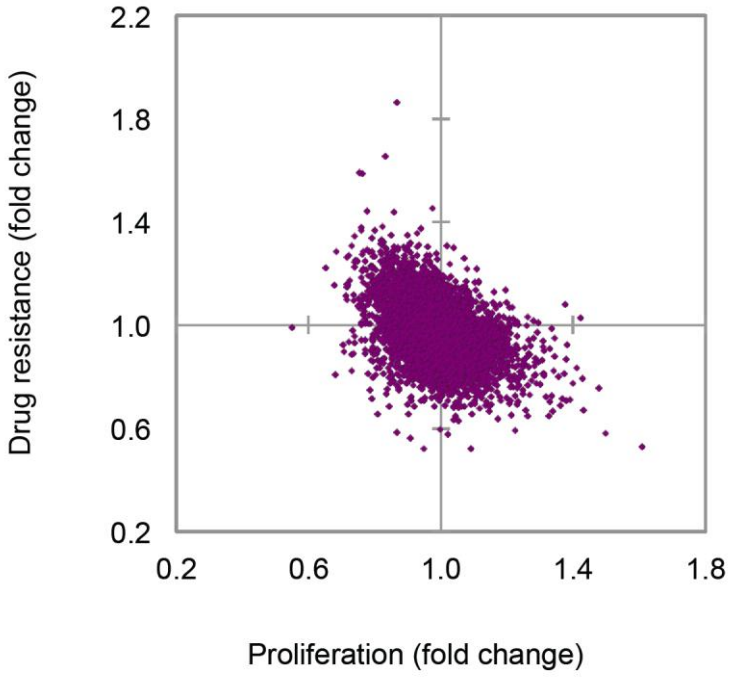

Supplementary Figure 12

Three-Wise miRNA Combinations Display Distinct Docetaxel Sensitivity and Anti-Proliferation Phenotypes.

Fold changes of normalized barcode counts for docetaxel (25 nM)-treated versus vehicle-treated OVCAR8-ADR cells (y-axis) and also for four-day versus one-day cultured cells (x-axis) were plotted for all three-wise miRNA combinations. Each data point represents the mean of two biological replicates.

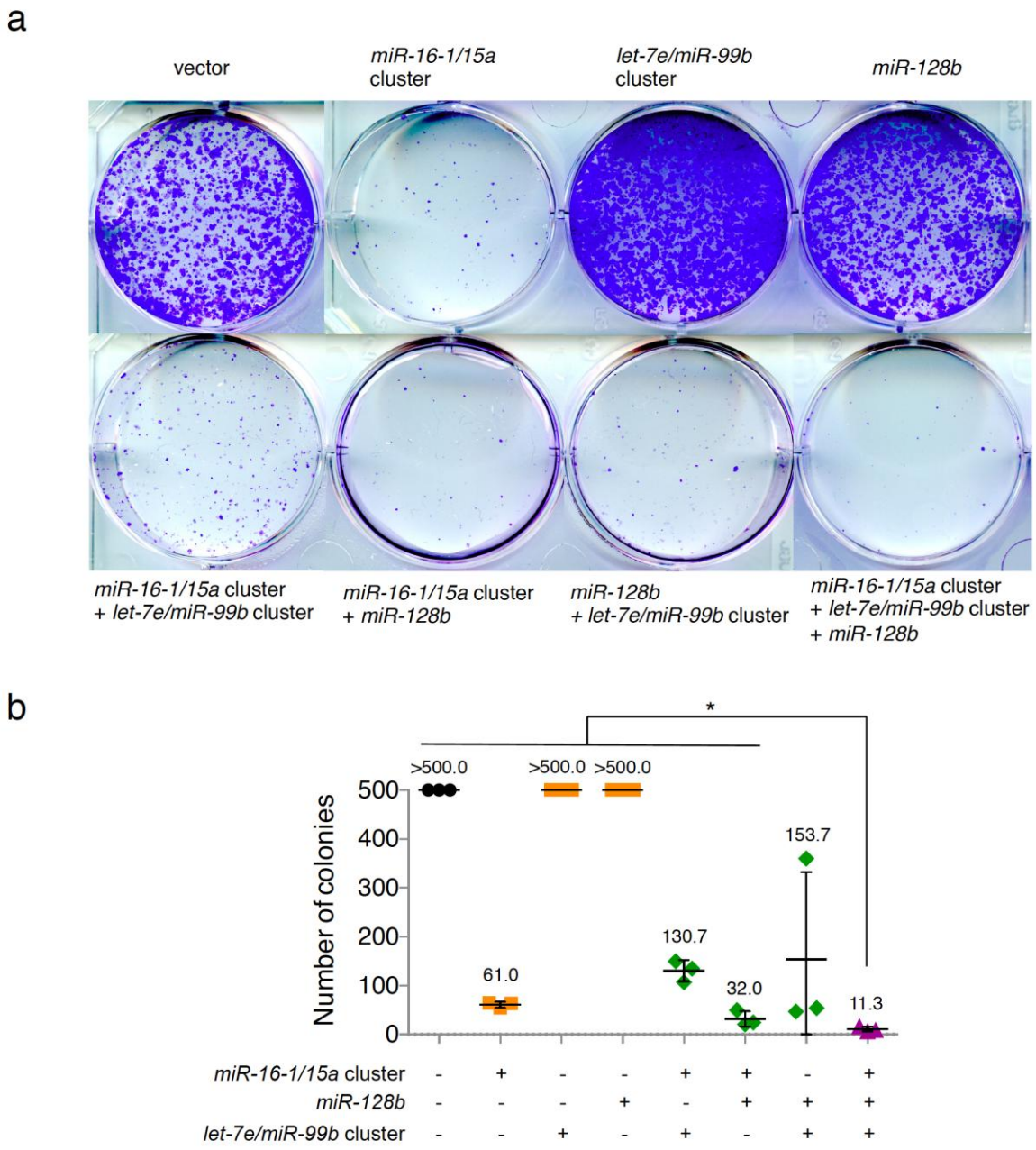

Supplementary Figure 13

Combinatorial Expression of the *miR-16-1/15a* Cluster, *miR-128b*, and the *let-7e/miR-99b* Cluster Inhibits Colony Formation by Viable OVCAR8-ADR Cells.

a, b, ~10,000 OVCAR8-ADR cells infected with each indicated miRNA combinations were treated with 25 nM of docetaxel for three days, and were cultured for another eleven days. Cells were stained with crystal violet to visualize colony formation for quantification. Representative images are shown in (**a**). The number of colonies for each sample was determined (**b**). The maximum number of discrete colonies that could be reliably counted was ~500 per well, and thus, samples with more than 500 colonies are presented as >500 colonies. Data represent mean ± s.d. (n = 3; *P < 0.05).

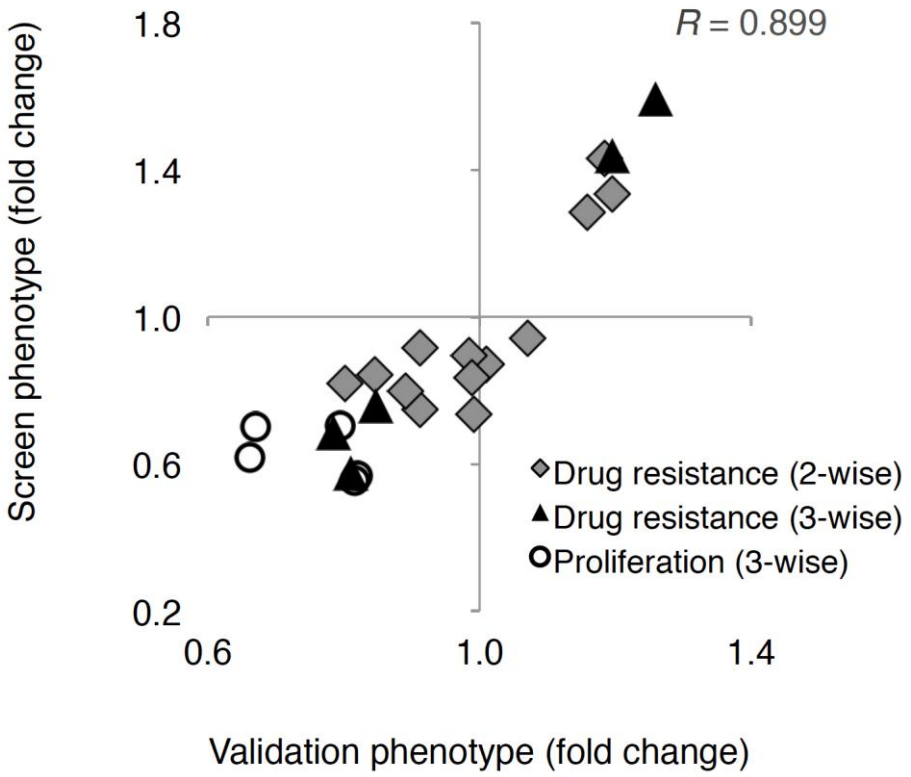

Supplementary Figure 14

High Consistency between Pooled Screens and Validation Data for Individual Hits.

For each two-wise and three-wise miRNA combination, the fold-change in the normalized barcode count for docetaxel (25 nM)-treated versus vehicle-treated OVCAR8-ADR cells, or four-day versus one-day cultured cells, obtained from the pooled screening data ('Screen phenotype') was plotted against its relative cell viability compared to vector control determined from the individual drug-sensitivity or cell-proliferation assays, respectively ('Validation phenotype') (R = 0.899). Data for the screening data are the mean of two biological replicates while the individual validation data represent the mean of three independent experiments. R is the Pearson correlation coefficient.

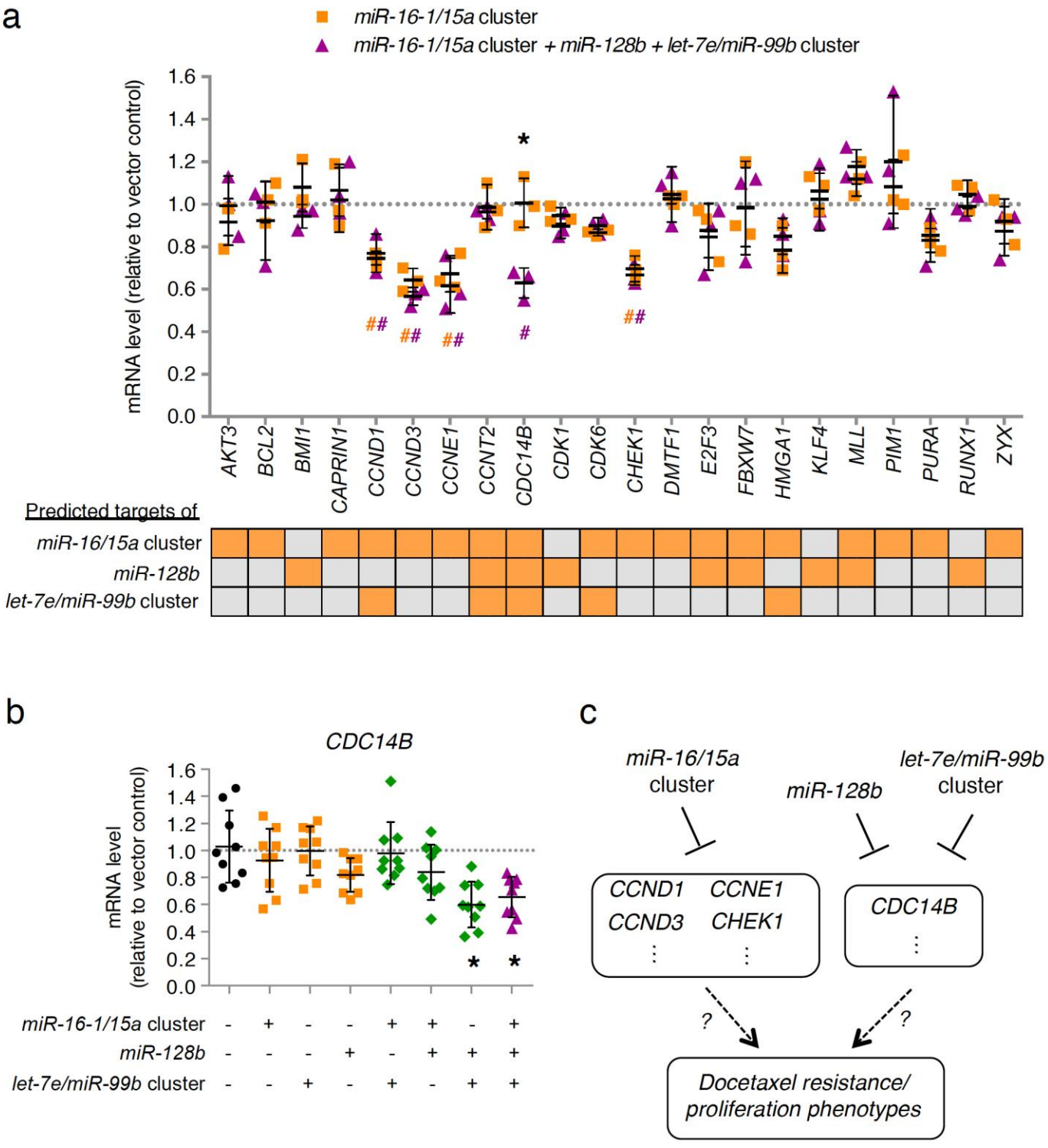

Supplementary Figure 15

Combinatorial Expression of the *miR-16/15a* Cluster, *miR-128b*, and/or the *let-7e/miR-99b* Cluster Reduce mRNA Levels of Targeted Genes in OVCAR8-ADR Cells.

a, qRT-PCR quantification of relative mRNA levels in OVCAR8-ADR cells expressing the *miR-16/15a* cluster or co-expressing the *miR-16/15a* cluster, *miR-128b*, and the *let-7e/miR-99b* cluster. Measured mRNA levels were normalized to *GAPDH* mRNA levels, and data represent mean ± s.d. (n = 3). mRNAs that were predicted or validated to contain conserved sites matching the seed region of the corresponding miRNAs using TargetScan and miRTarBase are shaded in orange in the table below the graph. Significant differences in the mRNA levels of *CCND1*, *CCND3*, *CCNE1* and *CHEK1* in cells expressing the *miR-16/15a* cluster (orange #; $P < 0.05$) or co-expressing the *miR-16/15a* cluster, *miR-128b*, and the *let-7e/miR-99b* cluster (purple #; $P < 0.05$) were determined by comparison with vector-control-infected cells. The asterisk (*$P < 0.05$) represents a significant difference in mRNA levels between cells expressing the *miR-16/15a* cluster versus co-expressing the *miR-16/15a* cluster, *miR-128b*, and the *let-7e/miR-99b* cluster. **b,** Relative mRNA levels of *CDC14B* in cells expressing various combinations of the *miR-16/15a* cluster, *miR-128b*, and/or the *let-7e/miR-99b* cluster. The mRNA level of *CDC14B* was significantly reduced in cells co-expressing the *let-7e/miR-99b* cluster and *miR-128b*, or the triple-combination expressing the *miR-16/15a* cluster, *miR-128b*, and the *let-7e/miR-99b* cluster. Data represent mean ± s.d. (n = 9; *$P < 0.05$). **c,** Summary diagram illustrating the potential roles of the *miR-16/15a* cluster, *miR-128b*, and the *let-7e/miR-99b* cluster in regulating the mRNA levels of multiple downstream targets. These genes may represent targets for future investigation into mechanisms that can modulate docetaxel resistance and/or proliferation phenotypes in OVCAR8-ADR cells.